J|A|C|S ARTICLES

Published on Web 02/20/2009

Specific Nucleotide Binding and Rebinding to Individual DNA Polymerase Complexes Captured on a Nanopore

Nicholas Hurt,[†] Hongyun Wang,[‡] Mark Akeson,[§] and Kate R. Lieberman*[,§]

Department of Chemistry and Biochemistry, Department of Applied Mathematics and Statistics, and Department of Biomolecular Engineering, Baskin School of Engineering, University of California, Santa Cruz, California 95064

Received December 10, 2008; E-mail: lieberman@biology.ucsc.edu

Abstract: Nanoscale pores are a tool for single molecule analysis of DNA or RNA processing enzymes. Monitoring catalytic activity in real time using this technique requires that these enzymes retain function while held atop a nanopore in an applied electric field. Using an α-hemolysin nanopore, we measured the dwell time for complexes of DNA with the Klenow fragment of *Escherichia coli* DNA polymerase I (KF) as a function of the concentration of deoxynucleoside triphosphate (dNTP) substrate. We analyzed these dwell time measurements in the framework of a two-state model for captured complexes (DNA−KF binary and DNA−KF−dNTP ternary states). Average nanopore dwell time increased without saturating as a function of correct dNTP concentration across 4 orders of magnitude. This arises from two factors that are proportional to dNTP concentration: (1) The fraction of complexes that are in the ternary state when initially captured predominantly affects dwell time at low dNTP concentrations. (2) The rate of binding and rebinding of dNTP to captured complexes affects dwell time at higher dNTP concentrations. Thus there are two regimes that display a linear relationship between average dwell time and dNTP concentration. The transition from one linear regime to the other occurs near the equilibrium dissociation constant (K_d) for dNTP binding to KF−DNA complexes in solution. We conclude from the combination of titration experiments and modeling that DNA−KF complexes captured atop the nanopore retain iterative, sequence-specific dNTP binding, as required for catalysis and fidelity in DNA synthesis.

Introduction

Nanoscale pores are a tool for single molecule analysis of DNA or RNA[1,2] and have been used to examine the interaction of nucleic acids with enzymes and binding proteins.[3−6] We recently showed that the α-hemolysin (α-HL) nanopore is sensitive to the functional state of captured enzyme complexes. Complexes of DNA with the Klenow fragment of *Escherichia coli* DNA polymerase I (KF) can be distinguished from DNA alone based upon current blockade amplitude. Complexes reside longer atop the nanopore when deoxynucleoside triphosphate (dNTP) complementary to the template base in the KF active site is present in the nanopore chamber.[7]

A single α-HL nanopore in a lipid bilayer is illustrated in Figure 1a. The pore vestibule can accommodate double-stranded (duplex) DNA, while the limiting aperture is only wide enough to accommodate single-stranded DNA.[8−10] Absent DNA, the open channel ionic current (I_o) through the α-HL pore is 60 pA at 180 mV applied potential in 0.3 M KCl. Voltage-dependent capture of a KF binary or ternary complex in the nanopore results in a decreased current (Figure 1b, i). This current reduction occurs when KF, which is too large to enter the pore vestibule, holds the duplex portion of the DNA substrate atop the pore, with the single-stranded template suspended in the pore lumen.[7] Upon voltage-promoted KF dissociation, the duplex DNA segment is drawn into the pore vestibule, causing a further current decrease (Figure 1b, ii). The amplitude and dwell time for this terminal current step are identical to capture events for the unbound DNA substrate.[7] The open channel current is restored following electrophoresis of the DNA through the pore (Figure 1b, iii). The dwell time and average amplitude for each current state are typically reported in nanopore experiments (Figure 1b−d).

Crystal structures of A-family polymerases related to KF reveal a conserved catalytic domain that resembles a partially open right-hand.[11] The palm subdomain contains residues

[†] Department of Chemistry and Biochemistry.
[‡] Department of Applied Mathematics and Statistics.
[§] Department of Biomolecular Engineering.

(1) Meller, A. *J. Phys.: Condens. Matter* **2003**, *15*, R582−R607.
(2) Kasianowicz, J. J.; Robertson, J. W. F.; Chan, E. R.; Reiner, J. E.; Stanford, V. M. *Annu. Rev. Anal. Chem.* **2008**, *1*, 737–66.
(3) Hendrickson, S. E.; Misakian, M.; Robertson, B.; Kasianowicz, J. J. *Phys. Rev. Lett.* **2000**, *85*, 3057–60.
(4) Kasianowicz, J. J.; Hendrickson, S. E.; Weetal, H. H.; Robertson, B. *Anal. Chem.* **2001**, *73*, 2268–72.
(5) Hornblower, B.; Coombs, A.; Whitaker, R. D.; Kolomeisky, A.; Picone, S. J.; Meller, A.; Akeson, M. *Nat. Methods* **2007**, *4*, 315–17.
(6) Cockroft, S. L.; Chu, J.; Amorin, M.; Ghadiri, M. R. *J. Am. Chem. Soc.* **2008**, *130*, 818–820.
(7) Benner, S.; Chen, R. J. A.; Wilson, N. A.; Abu-Shumays, R.; Hurt, N.; Lieberman, K. R.; Deamer, D. W.; Dunbar, W. B.; Akeson, M. *Nat. Nanotechnol.* **2007**, *2*, 718–724.
(8) Song, L.; Hobaugh, M. R.; Shustak, C.; Cheley, S.; Bayley, H.; Gouaux, J. E. *Science* **1996**, *274*, 1859–866.
(9) Kasianowicz, J. J.; Brandin, E.; Branton, D.; Deamer, D. W. *Proc. Natl. Acad. Sci. U.S.A.* **1996**, *93*, 13770–73.
(10) Vercouture, W.; Winters-Hilt, S.; Olsen, H.; Deamer, D.; Haussler, D.; Akeson, M. *Nat. Biotechnol.* **2001**, 248–52.
(11) Brautigam, C. A.; Steitz, T. A. *Curr. Opin. Struct. Biol.* **1998**, *8*, 54–63.

10.1021/ja809663f CCC: $40.75

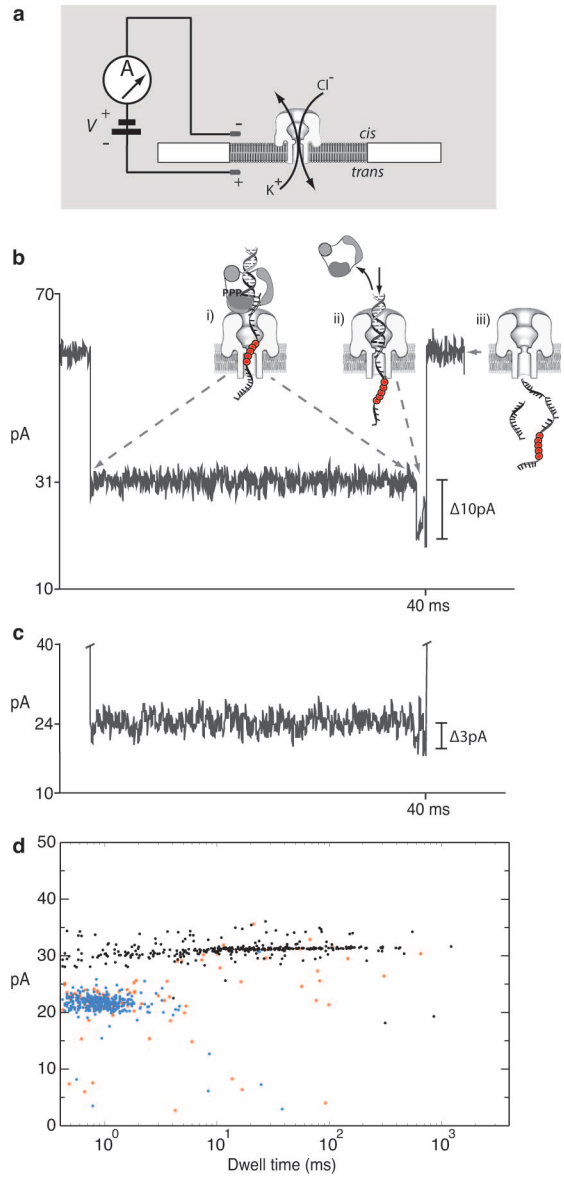

Figure 1. Detection of capture events with the nanopore device. (a) Schematic of the nanopore device. A patch-clamp amplifier supplies voltage and measures ionic current through a single α-HL channel inserted in a ~25-μm diameter lipid bilayer (trans-side positive). Current through the nanopore is carried by K^+ and Cl^- ions. (b) Representative current trace at 180 mV and 23 °C for nanopore capture of a ternary complex of KF, dGTP, and the 5ab(12,16) 14 bphp DNA substrate. Cartoons in b illustrate the molecular events that correspond to each current level. Red circles in the DNA strand represent the segment of five abasic residues in the 5ab(12,16) 14 bphp. A dNTP molecule is illustrated with its nucleobase base-paired to the $n = 0$ template position in the KF active site, and its triphosphate moiety indicated as −PPP. (i) The initial long blockade at 31 pA is the enzyme bound state (EBS). It arises from capture of binary or ternary complex, with the duplex DNA held atop the pore vestibule because of association with KF. (ii) The shorter ~21 pA terminal step occurs when KF dissociates and the duplex DNA drops into the nanopore vestibule. (iii) The DNA hairpin unfolds and translocates through the nanopore, resulting in a return to the open channel current. (c) Representative current trace for capture of a ternary complex of KF, dGTP, and the standard DNA 14 bphp substrate. The amplitude of the initial blockade corresponding to the EBS with the standard DNA substrate is 24 pA. (d) Dwell time vs amplitude plot showing the EBS current segments (black points) and their corresponding terminal current step segments (blue points) for a representative experiment in which 1 μM DNA (5ab(12,16) 14 bphp), 2 μM KF, and 4 μM dGTP were present in the nanopore chamber. The red points indicate events that lack terminal current steps.

essential for catalysis, the thumb subdomain positions the primer/template DNA duplex in the active site, and the fingers subdomain is essential for binding the incoming dNTP substrate. Binary and ternary complex structures reveal a conformational transition between these two functional states.[12−14] In ternary complexes, the fingers subdomain rotates toward the active site to achieve a tight steric fit with the nascent base pair. In this closed complex, the affinity of KF for its DNA substrate is increased by ~5- to 8-fold.[15]

Polymerase-catalyzed DNA strand extension was recently measured using an α-HL nanopore.[6] In that study, substrate binding and catalysis occurred in the bulk phase, and the extension product was subsequently detected when it was drawn back onto the nanopore by a voltage reversal. To observe and measure synthesis in real time, our goal is to monitor polymerase activity while the enzyme is coupled to DNA atop the nanopore under applied voltage. To achieve this, individual polymerase molecules must retain the ability to iteratively bind substrates and release products while they are held against the surface of the nanopore.

In the current study, we have examined nanopore dwell time for DNA−KF complexes as a function of dNTP concentration. Using a DNA substrate bearing a 2′,3′-dideoxy terminus that prevents catalytic turnover but allows closed ternary complex formation in response to the correct incoming dNTP,[12,13,16] we demonstrate reversible, iterative, sequence-specific binding of dNTP substrate from the bulk phase to complexes of KF and DNA while they are captured atop the nanopore.

Results

Effect of KF Concentration on DNA−KF Capture Events. In order to reliably detect and quantify DNA−KF complexes captured in the nanopore, we used a 14 base-pair hairpin (14 bphp) DNA with a 35 residue single-stranded overhang that contained a block of five abasic (1′,2′-dideoxy) residues (Figure S1). Upon the basis of the dimensions of the nanopore[8] and the length of single-stranded DNA, these abasic residues were placed so that when bound to KF with the complex perched atop the nanopore, the abasic segment resides in the nanopore lumen (Figure 1b, i). We predicted that this abasic substrate would allow more ionic current in the enzyme-bound state (EBS) than would a substrate with standard DNA residues. Consistent with this, median amplitude of the measured ionic current for the EBS was 31 pA for the 5ab(12,16) substrate (Figure 1b, i) and 24 pA for an otherwise identical standard DNA substrate (Figure 1c). By enhancing the amplitude difference between the EBS and the terminal step (21 pA), the abasic substrate allows reliable detection and quantification of the EBS, even when it is of short duration (Figure 1b,d).

We tested the effect of KF concentration on the capture of DNA−KF complexes (Table 1). When KF was titrated into the nanopore cis chamber in the presence of 1 μM 14 bphp, the percentage of DNA molecules captured as DNA−KF binary complexes increased with enzyme concentration. However, the nanopore dwell time of the captured binary complexes was

(12) Doublié, S.; Tabor, S.; Long, A. M.; Richardson, C. C.; Ellenberger, T. *Nature* **1998**, *391*, 251–58.
(13) Li, Y.; Korolev, S.; Waksman, G. *EMBO. J.* **1998**, *17*, 7514–525.
(14) Johnson, S. J.; Taylor, J. S; Beese, L. S. *Proc. Natl. Acad. Sci. U.S.A.* **2003**, *100*, 3895–3900.
(15) Joyce, C. M.; Potapova, O.; Delucia, A.; Huang, X.; Basu, V.; Grindley, N. D. F. *Biochemistry* **2008**, *47*, 6103–116.
(16) Dzantiev, L.; Romano, L. J. *Biochemistry* **2000**, *39*, 356–361.

Table 1. Effect of KF Concentration on Capture of DNA−KF Complexes in the Nanopore[a]

KF (μM)	total events[b]	% of events with EBS[c,d]	EBS median dwell time (ms)[d]	95% confidence interval of median (ms)[e]
0	231	1.7	–	–
0.25	223	22.4	1.8	(1.3, 2.6)
0.5	479	28.8	2.5	(2.0, 2.65)
1	407	36.1	1.9	(1.6, 2.2)
1.5	371	54.4	2.0	(1.6, 2.3)
2	323	55.7	1.85	(1.6, 2.1)
3	120	59.2	2.2	(1.7, 3.0)

[a] KF was added at the indicated concentrations to the nanopore *cis* chamber in the presence of 1 μM 5ab(12,16) 14 bphp DNA. [b] Capture events were measured at 180 mV applied potential and identified as described in Methods. [c] EBS, enzyme-bound state. [d] Events with an EBS and terminal step were identified and their dwell times were quantified as described in Methods. [e] See Section 5 of the Supporting Information for statistical analysis and Table S3 for the key statistical quantities of the EBS dwell time distributions.

unaffected by KF concentration (Table 1). This indicates that KF does not rebind to individual DNA molecules while they are captured in the pore, consistent with the sequence of events in the model shown in Figure 1b. Upon KF dissociation, the duplex DNA is drawn into the nanopore vestibule, where the double strand−single strand DNA junction recognized by the polymerase becomes inaccessible.

Effect of dGTP Concentration on DNA−KF Capture Events. In contrast to the results above for the KF titration, we showed previously that the presence of correct incoming dNTP increased the nanopore dwell time of DNA−KF complexes.[7] To further examine this effect, we titrated dGTP (complementary to the dCMP template base in the KF active site) into the nanopore chamber containing 2 μM KF and 1 μM DNA. The 14 bphp DNA substrate bears a 2′,3′-dideoxy terminus to prevent catalytic dNTP incorporation. Each nanopore event reports capture, retention until KF dissociation, and subsequent translocation through the pore for a single DNA molecule. Therefore these titrations assay the effect of dGTP on the resistance of captured complexes to voltage-promoted enzyme dissociation.

The titration experiments revealed a dGTP concentration-dependent increase in dwell times that appears unsaturated over 4 orders of magnitude in dGTP concentration. Histograms of log dwell time distribution are shown in Figure 2. Binary complexes (0 μM dGTP) show a well defined distribution centered at 2 ms (Figure 2, top panel). As dGTP is titrated into the chamber, a second peak emerges centered at 30 ms. Between 0 and 15 μM, increasing dGTP causes the binary complex peak to recede while the peak at 30 ms, attributable to ternary complexes, increases. However, at dGTP concentrations above 15 μM, a change in behavior occurs (Figure 2, 15−10 000 μM panels). The peak at 2 ms corresponding to binary complex is depleted, and the dGTP-dependent peak shifts to longer dwell times as the dGTP concentration is increased. This shift continues without reaching saturation up to 10 000 μM dGTP, the highest concentration that was tested.

The ability of dNTP to elicit long dwell times was dependent upon complementarity to the template base in the KF active site. Median dwell times (with 95% confidence intervals in parentheses after each value) for the EBS of captured DNA−KF complexes in the presence of 100, 500, and 3000 μM dTTP were 2.2 (1.6, 2.6), 2.4 (2.1, 2.9), and 2.85 (2.2, 3.7) ms, respectively (Table S2, Supporting Information). These represent very small increases over the median dwell time for DNA−KF

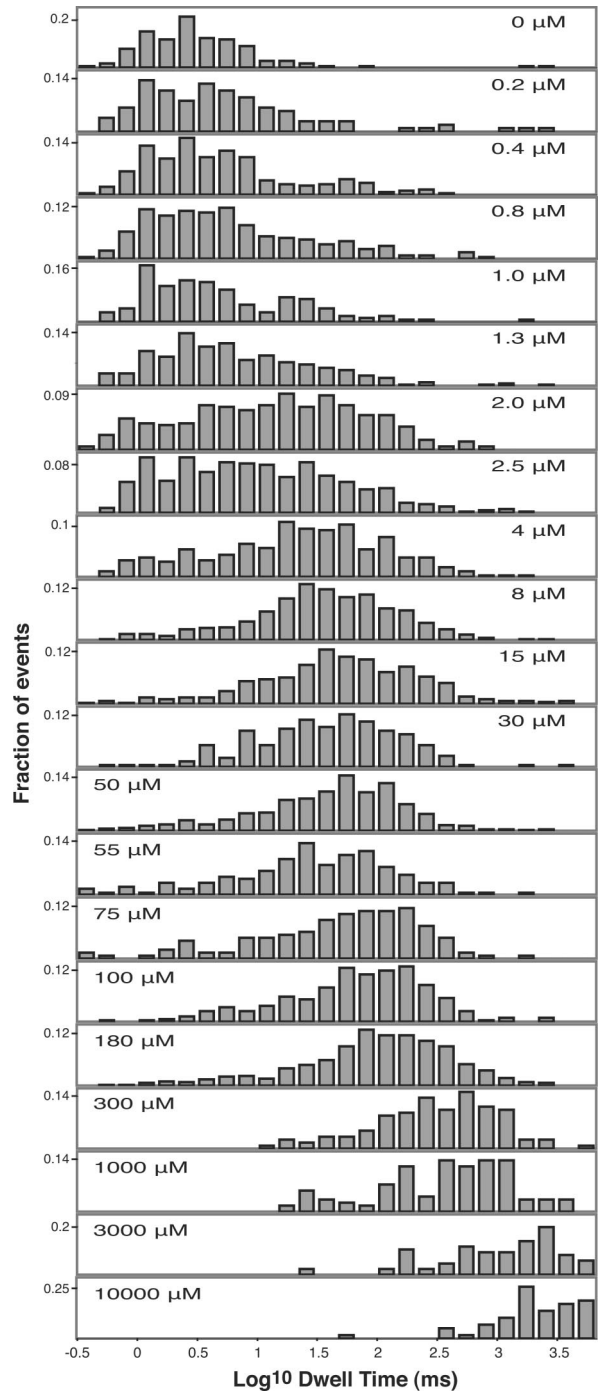

Figure 2. Effect of dGTP concentration on nanopore dwell time of captured DNA−KF complexes. Histograms of log dwell time (in ms) are shown for the EBS of nanopore capture events measured in experiments with the 5ab(12,16) 14 bphp DNA substrate (1 μM), KF (2 μM), and dGTP at the concentrations indicated in the figure panels. The histograms for dGTP concentrations from 0 μM to 1000 μM represent no less than 105, and up to 653, EBS events (Table S1, Supporting Information). Data for dwell times longer than 4700 ms is not displayed in the histograms for 3000 μM dGTP (89 total EBS events) and 10 000 μM dGTP (69 total EBS events) because of space limitations. See the Supporting Information for the calculation of the 95% confidence interval for the observed number of samples in each individual bin of the histograms, and plots of histograms with error bars (representing 95% confidence intervals) for sixteen dGTP concentrations (Figures S5−S8, Supporting Information).

binary complexes (0 μM dNTP) of 1.9 (1.6, 2.1) ms. Moreover, the median dwell time promoted by 3000 μM dGTP of 965.1 (625.8, 1218) ms (Table S1, Supporting Information) is >300

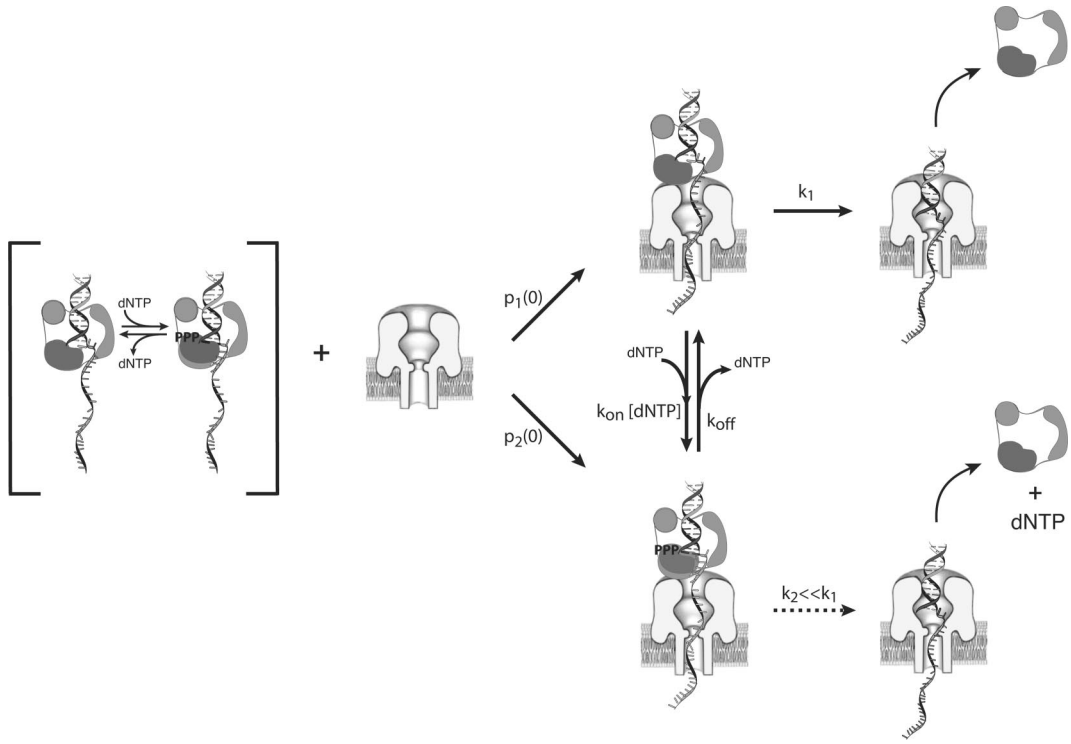

Figure 3. Two-state model for dNTP binding to DNA−KF complexes captured in the nanopore. Illustration of a model for two states of nanopore-captured DNA−KF complexes (binary and ternary) and the probabilities and rates that govern transitions to and from these two states. Probabilities of initial capture of either binary or ternary complex are indicated as $p_1(0)$ and $p_2(0)$, respectively, and are dependent upon the bulk phase equilibrium of binary and ternary complexes. Captured complexes can exchange between the binary and ternary states while they reside atop the pore because of dNTP binding (k_{on}[dNTP]) and unbinding (k_{off}). KF dissociates (k_1) only from binary complexes. KF dissociation is irreversible because the double strand-single strand DNA junction drops into the nanopore vestibule where it is inaccessible to KF.

times longer than observed in the presence of dTTP at the same concentration.

We hypothesized that DNA−KF complexes captured atop the nanopore are able to bind, unbind, and rebind dNTP. In the presence of dGTP, either binary or ternary complexes are captured. The relative capture frequency for each species reflects their abundance in the bulk phase. At low dGTP concentrations, when binary complex is captured, KF dissociates rapidly, ending the event. We propose that the unsaturated increase in dwell time in response to high dGTP concentrations indicates that KF rarely dissociates directly from captured ternary complexes. Therefore, when ternary complexes are captured at low dGTP concentrations, they reside atop the nanopore until dGTP dissociates. This yields binary complex, from which KF rapidly dissociates, ending the event. Hence at low dGTP concentrations, two peaks corresponding to binary (2 ms) and ternary (30 ms) complexes are observed in the histograms of log dwell time (Figure 2, 0−15 μM panels).

When the dGTP concentration is high enough to yield dGTP association rates that exceed the rate of KF dissociation in the binary state, it is more likely that dGTP will bind to captured binary complexes before KF dissociation can occur. This yields the ternary state. At high dGTP concentrations, the captured complex can fluctuate many times between the binary state and the ternary state before KF dissociation. Binding and rebinding to complexes while they are perched atop the nanopore occurs with increasing probability as the dGTP concentration is increased. This results in the unsaturated, dGTP concentration-dependent shift to longer dwell times observed in the histograms (Figure 2, 15−10 000 μM panels).

Mathematical Model. To further examine this hypothesis, we developed a mathematical model that posits two states for captured DNA−KF complexes, binary (absent dGTP) and ternary (dGTP bound). In this model we examine probabilities and rates of transition to, from, and between these two states, their dependence upon dGTP concentration, and the effect of these parameters on dwell time of the EBS in the nanopore. This model is illustrated in Figure 3. Kinetic models of similar forms have been used in studying open-closed durations in ion channel gating.[17]

The initial probability of a captured complex being in the binary state is denoted by $p_1(0)$ while the initial probability of a captured complex being in the ternary state is $p_2(0)$. These probabilities are a function of the binding affinity of dGTP for the binary complex in bulk solution $K_d^{(B)}$ and are thus dGTP concentration dependent. A complex captured in the ternary state could either release dGTP (k_{off}) leaving a binary complex atop the pore, or KF and dGTP could dissociate from DNA directly from the ternary complex (k_2). Because of the unsaturated increasingly long dwell times at high dGTP concentrations we assume k_2 to be negligible in this model. Thus, transition to the binary state is the predominant pathway to KF dissociation for captured ternary complexes. A captured complex that is in the binary state could either bind dGTP (k_{on} [dGTP]), or KF could dissociate from DNA (k_1). These two possible transitions for binary complexes are in competition. The rate of KF dissociation, k_1, is constant while the dGTP binding rate, k_{on} [dGTP], increases with dGTP concentration. The binding affinity of dGTP for the binary complex while captured atop the nanopore is a ratio of k_{off}/k_{on} and is denoted by K_d. In our model, K_d for captured complexes atop of the pore and $K_d^{(B)}$ for complexes

(17) Popescu, G.; Auerbach, A. *Nat. Neurosci.* **2003**, *6*, 476–83.

in solution are two different model parameters; we do not assume that $K_d = K_d^{(B)}$.

The transition rates defined above can be used to derive an equation (see Supporting Information) for mean EBS dwell time:

$$\langle T\rangle = \frac{1}{k_1} + \frac{[\mathrm{dGTP}]}{K_d} \times \frac{1}{k_1} + \frac{\dfrac{[\mathrm{dGTP}]}{K_d^{(B)}}}{\dfrac{[\mathrm{dGTP}]}{K_d^{(B)}} + 1} \times \frac{1}{k_{off}} \qquad (1)$$

There are four kinetic or equilibrium constants in this equation: $\{k_1, K_d^{(B)}, K_d, k_{off}\}$. To determine the values of these four parameters, we use the experimental data for several of the lowest and highest dGTP concentrations.

For low dGTP concentrations, or more specifically when $[\mathrm{dGTP}]/K_d^{(B)} \ll 1$, the mean dwell time is well approximated by a linear function:

$$\langle T\rangle = [\mathrm{dGTP}]\left(\frac{1}{K_d k_1} + \frac{1}{K_d^{(B)} k_{off}}\right) + \frac{1}{k_1}$$

We fit the experimental data for low dGTP concentrations to a linear function using the least-squares formulation on a linear scale (Figure 4a). Let s_1 be the slope of the line and y_1 be the vertical intercept of the line. We have:

$$\begin{cases} \dfrac{1}{K_d k_1} + \dfrac{1}{K_d^{(B)} k_{off}} = s_1 \\ \dfrac{1}{k_1} = y_1 \end{cases} \qquad (2)$$

For high dGTP concentrations, when $[\mathrm{dGTP}]/K_d^{(B)} \gg 1$, the mean dwell time is well approximated by another linear function:

$$\langle T\rangle \approx [\mathrm{dGTP}] \times \frac{1}{K_d k_1} + \left(\frac{1}{k_{off}} + \frac{1}{k_1}\right)$$

We fit the experimental data for high dGTP concentrations to a linear function using the least-squares formulation on a logarithmic scale (Figure 4b). Let s_2 be the slope of the line and y_2 be the vertical intercept of the line. We have:

$$\begin{cases} \dfrac{1}{K_d k_1} = s_2 \\ \left(\dfrac{1}{k_{off}} + \dfrac{1}{k_1}\right) = y_2 \end{cases} \qquad (3)$$

The four parameters are then determined from the experimental data using the following equations:

$$k_1 = \frac{1}{y_1} \qquad k_{off} = \frac{1}{y_2 - y_1} \qquad K_d = \frac{y_1}{s_2} \qquad K_d^{(B)} = \frac{y_2 - y_1}{s_1 - s_2}$$

From the low concentration mean dwell time data, we used the first four data points to determine the slope $s_1 = 10.4$ (6.77, 14.1) and the intercept $y_1 = 3.45$ (2.49, 4.41). The pair of parentheses immediately after each estimated value contains the 95% confidence interval for that model parameter (see section 5.3 of the Supporting Information for uncertainty estimations). From the high concentration data, we used the last six data points to determine the slope $s_2 = 0.459$ (0.048, 0.507) and the intercept $y_2 = 45.2$ (33.6, 56.5). Using these slopes and intercepts to calculate the four parameters, we arrive at $k_1 = 290\ \mathrm{s}^{-1}$ (227, 402), $k_{off} = 23.9\ \mathrm{s}^{-1}$ (18.8, 33.1), $K_d = 7.52\ \mu\mathrm{M}$ (6.81, 8.46), and $K_d^{(B)} = 4.20\ \mu\mathrm{M}$ (2.72, 6.89). Thus the value of $k_{on} = k_{off}/K_d = 3.18\ \mu\mathrm{M}^{-1}\ \mathrm{s}^{-1}$ (2.29, 4.71).

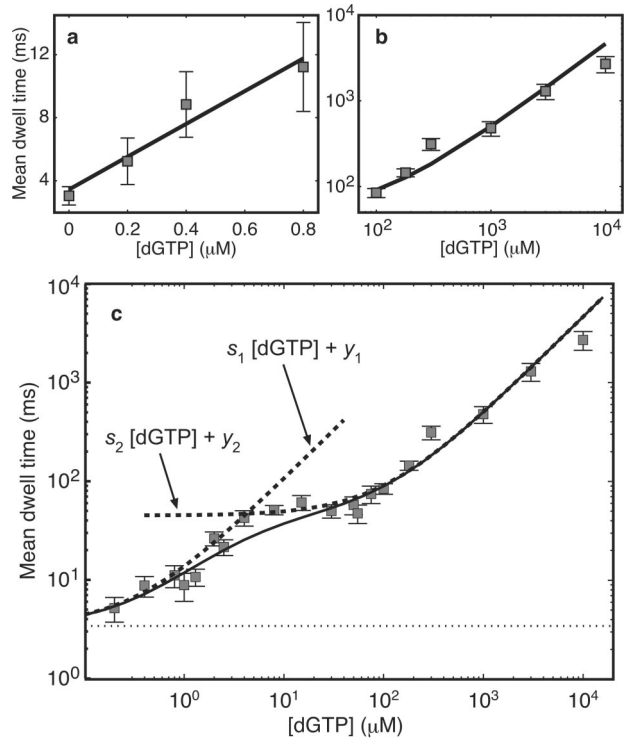

Figure 4. Comparison of dGTP concentration-dependent EBS mean dwell times predicted by the model and the experimentally observed mean dwell times. (a) EBS mean dwell times measured for the four lowest dGTP concentrations ($[\mathrm{dGTP}] \ll K_d^{(B)}$) were fit to a linear function using the least-squares formulation. (b) EBS mean dwell times measured for the six highest dGTP concentrations ($[\mathrm{dGTP}] \gg K_d^{(B)}$) were fit to another linear function using the least-squares formulation on a logarithmic scale. Slopes and y-axis intercept values from (a) and (b) were used to determine kinetic parameters k_1, k_{off}, K_d, and $K_d^{(B)}$. (c) Experimentally observed mean dwell times (squares) and those predicted from a model generated using the kinetic parameters (solid line). The dGTP-concentration dependence of the measured and predicted mean dwell times across the entire range of dGTP concentrations tested is shown. The dashed lines show the two linear functions from a and b (which are not straight lines when plotted in log−log scale). The model curve shows the transition from one linear function to the other, which occurs in a region around $[\mathrm{dGTP}] = K_d^{(B)}$. Error bars indicate the 95% confidence interval for each sample mean. The dotted line indicates the experimental mean dwell time for the binary complex of KF and DNA (0 μM dGTP).

Comparison of the Model Results and Experimental Results. Inserting the values of the four parameters into eq 1 allows us to predict the mean dwell time for the EBS over the full range of dGTP concentrations. The mean dwell times determined by mathematical modeling are consistent with the experimentally observed mean dwell times (Figure 4c), which were estimated by averaging the observed dwell time samples for each dGTP concentration (Figure 4). The error bars show 95% confidence intervals, which were estimated from the sample variance of dwell time and the number of dwell time samples at each concentration (for mathematical details of the calculation, see Supporting Information). While the model curve is within the error bars for the majority of dGTP concentrations, it is outside the confidence interval for a few of the data points (Figure 4c). It is important to note that the error bars represent only the statistical uncertainty and cannot account for potential variation from other experimental factors. Nonetheless, the model is consistent with overall trend of the experimental data across a range of both dGTP concentrations and dwell times spanning 4 orders of magnitude.

The model curve, which was generated using data limited to low (Figure 4a) and high (Figure 4b) dGTP concentrations, features a transition region around [dGTP] = $K_d^{(B)} = 4.20\ \mu$M. This region reveals the transition from the linear function for low dGTP concentrations (s_1[dGTP] + y_1) to the linear function for high dGTP concentrations (s_2[dGTP] + y_2). This transition region is also observed in the experimental data, although it is sharper than in the model curve (Figure 4c). In the dGTP concentration regime in which this transition occurs, the fraction of complexes initially captured in the ternary state goes from small to saturation, while the effect of dGTP binding and rebinding to captured complexes goes from negligible to dominant. Here a log−log plot is adopted to accommodate the wide range of dGTP concentrations and mean dwell times in the experimental data. However, in a log−log plot, a linear function does not appear as a straight line, which makes it difficult to see the transition from one linear function to the other. To illustrate the transition, in Figure 4c we also plot the two linear functions obtained in Figure 4a and 4b: s_1[dGTP] + y_1 for low dGTP concentrations and s_2[dGTP] + y_2 for high dGTP concentrations. Notice that these two linear functions intersect at [dGTP] = $(y_2 - y_1)/(s_1 - s_2) = K_d^{(B)}$ (see Supporting Information). It is in this transition region that the population distributions of log dwell time shift from two peaks that change in their relative populations (Figure 2, 0−15 μM panels) to a single dGTP-dependent peak with continuously increasing dwell time (Figure 2, 15−10 000 μM panels). We thus conclude that the transition from one linear function to the other in both the modeled and experimental curves is attributable to the increasing influence of binding and rebinding of dGTP to the captured complex on the dwell time in the EBS.

After the transition region, mean dwell time increases linearly with dGTP concentration. The model indicates that this is due to a dGTP concentration-dependent increase in the number of rebinding cycles for individual complexes captured on the nanopore. This in turn leads to a decrease in the fraction of time that the complex is in the binary state, from which there is a constant rate of enzyme dissociation (k_1). We would expect the ability of dGTP to promote longer dwell times to saturate once the dwell time approaches the reciprocal of the rate of enzyme dissociation from the ternary complex. We did not observe such saturation, even at the highest dGTP concentrations that could be tested. This supports the assumption that dissociation of KF directly from captured ternary complexes (k_2) is negligible.

The titration data were plotted as a function of the amount of dGTP added to the nanopore cis chamber, which is not the same as the concentration of free dGTP in solution. We examined the deviation of these values, which could lead to potential misrepresentation of the relationship between dwell time and dGTP concentration, particularly at lower dGTP concentrations. Posterior analysis, using values for the binding affinity of dGTP for the binary complex and the binary complex concentration at equilibrium, showed that at the very lowest dGTP concentrations, 87.5% of the initial input dGTP is free in solution (Table 2; Figure S3, Supporting Information). This percentage converges toward 100% as dGTP concentration increases, with 94.4% and 99.9% free dGTP for 10 and 1000 μM initial dGTP, respectively. Thus the input dGTP concentration is a good approximation of free dGTP in solution.

Table 2. Posterior Analysis of Free dGTP Concentrations[a]

initial dGTP concentration (μM)	concentration of free dGTP at equilibrium (μM)	free dGTP as a fraction of initial dGTP, %
0.01	0.00875	87.5
0.1	0.0876	87.6
0.3	0.264	87.9
1	0.888	88.8
3	2.73	90.9
10	9.44	94.4
100	99.1	99.1
1000	999.0	99.9

[a] Posterior analysis on the concentration of free dGTP in solution at each inital dGTP concentration in the titration experiments was conducted as described in the Supporting Information, using values for the binding affinity of dGTP for the DNA−KF binary complex and the binary complex concentration at equilibrium.

Discussion

We have used a combination of titration experiments and modeling to demonstrate that DNA−KF complexes retain the ability to bind, release, and rebind dNTP substrates while they are held atop the α-HL nanopore under applied voltage. Maintenance of polymerase function in this configuration is a prerequisite for most strategies to monitor DNA synthesis in real time using nanopores. To observe multiple rounds of catalytic nucleotide addition, it is also necessary that binary complexes remain on the pore without dissociating long enough to allow dNTP to bind for each catalytic cycle. Our data indicate that both of these requirements are met, permitting the use of the nanopore as a tool for the single molecule study of DNA polymerases as molecular motors, as well as for DNA sequencing schemes that rely upon enzymes coupled with sensors within the nanopore.[18]

The K_d values determined from mathematical modeling for the captured (7.52 μM) and bulk phase (4.2 μM) complexes are close to one another and in agreement with the K_d determined for dNTP binding to DNA−KF complexes (5 μM) in pre-steady-state kinetic studies.[19] This indicates that the active site of captured KF complexes remains largely undistorted. Reversible, iterative dNTP binding also implies that KF can transition between open and closed conformers atop the pore.

KF ternary complex assembly follows an ordered mechanism in which KF first binds to DNA, followed by dNTP binding to the binary complex.[20] The data and model in this study support the proposal that voltage-promoted KF dissociation occurs from the binary complex, regardless of whether binary or ternary complex was initially captured. Ternary complexes captured on the pore under voltage thus dissociate via a reversal of the obligate ordered assembly pathway, further evidence of their functional integrity.

In bulk phase, the DNA−KF binary complex is in rapid equilibrium between open and closed conformers.[21,22] Initial

(18) Wu, H. C.; Astier, Y.; Maglia, G.; Mikhailova, E.; Bayley, H. *J. Am. Chem. Soc.* **2007**, *129*, 16142–48.
(19) Kuchta, R. D.; Mizrahi, V.; Benkovic, P. A.; Johnson, K. A.; Benkovic, S. J. *Biochemistry* **1987**, *26*, 8410–17.
(20) Dahlberg, M. E.; Benkovic, S. J. *Biochemistry* **1991**, *30*, 4835–843.
(21) Purohit, V.; Grindley, N. D.; Joyce, C. M. *Biochemistry* **2003**, *42*, 10200–211.
(22) Rothwell, P. J.; Mitaksov, V.; Waksman, G. *Mol. Cell* **2005**, *19*, 345–355.

binding of dNTP to the open conformer is mediated largely through recognition of the triphosphate moiety,[23] affording minimal discrimination against incorrect dNTPs. If the tight active site steric fit achieved by the binding of correct dNTP is detected when the closed conformation is sampled, the conformational equilibrium is shifted strongly toward the closed state. This enables active site rearrangements that are rate-limiting for catalysis.[15,21]

Crystal structures[12,14] and biochemical experiments[16,21] have provided strong evidence that in the presence of correct incoming dNTP, DNA polymerase ternary complexes with dideoxy-terminated primers achieve the stabilized closed conformation, despite the absence of the primer 3′-OH. The complexes we have studied therefore access the steps in the KF reaction pathway that occur prior to the chemical step of nucleotide incorporation.[15,21] We found that incorrect dNTP, even at high concentrations, did not support nanopore dwell times longer than those of binary complexes. This indicates that the increase in nanopore dwell times elicited by correct dNTP is due to specific interactions in the KF active site and that the unsaturated increase in dwell time at high dGTP concentrations is due to dNTP binding, unbinding, and rebinding rather than nonspecific or off-pathway processes. We conclude that DNA−KF complexes captured atop the nanopore undergo reversible, sequence-specific dNTP binding. This specific substrate recognition is a hallmark of biological catalysis and a requirement for fidelity in DNA synthesis.

Methods

Materials. The 5ab(12,16) 14 bphp DNA oligonucleotide was synthesized by Stanford University Protein and Nucleic Acid Facility using D-spacer phosphoramidites (Glen Research) and was purified by denaturing PAGE. The sequence is shown below, with each abasic (1′,2′-dideoxy) residue indicated by an X, and the complementary regions of the hairpin stem underlined:

5′-ACT ATC ATT ATC TAC ATC XXX XXC ATC ACT ACT CCG CAT GCA GGT AGC CTT TTG GCT ACC TGC ATG ddC-3′.

An oligonucleotide identical to the 5ab(12,16) 14 bphp except for the region of abasic residues was used in preliminary experiments (Figure 1c). The sequence is:

5′-ACT ATC ATT ATC TAC ATC CAT TAC ATC ACT ACT CCG CAT GCA GGT AGC CTT TTG GCT ACC TGC ATG ddC−3′.

The 3′ terminal residue of both DNA substrates was 2′,3′-dideoxycytidine (ddC), enabling ternary complex formation without catalytic turnover. The $n = 0$ template base for both substrates was C; thus, the complementary incoming nucleotide was dGTP. Prior to use, DNA substrates were denatured at 95 °C for 2 min and quickly annealed in ice−water to prevent intermolecular hybridization.

Klenow fragment (exo) was obtained from New England Biolabs (100 000 U ml^{-1}; specific activity 20 000 U mg^{-1}). Deoxynucleoside triphosphates (dNTPs) were from GE Healthcare Life Sciences.

Nanopore Methods. The setup of the nanopore chamber and insertion of a single α-HL nanopore have been described.[24,25] Ionic current flux through the α-HL channel was measured using an Axopatch 200B integrating patch-clamp amplifier (Molecular Devices) in voltage-clamp mode. Data were acquired with a Digidata 1440A analog-to-digital converter (Molecular Devices) at 20 μs intervals in the whole cell configuration, and filtered at 10 kHz using a low-pass Bessel filter. Current blockades were examined at 180 mV (trans-positive) for the voltage-clamped experiments.

Experiments were conducted at 23 ± 0.2 °C in 10 mM HEPES/KOH, pH 8.00 ± 0.05, 0.3 M KCl, 5 mM $MgCl_2$, conditions shown to support KF catalytic function[3] and to optimize current blockade detection. With DNA (1 μM) present, KF and dNTP were added to the nanopore cis chamber at the concentrations indicated in the table and figures. All dNTP titration experiments were conducted in the presence of 2 μM KF.

Data Analysis. Current blockades events were identified using MATLAB (2007a, The MathWorks, Natick, MA) and software developed in our laboratory. An event was identified when the current level dropped from the open channel current (∼60 pA at 180 mV) by at least 8 pA for at least 0.2 ms. To quantify the EBS and terminal steps of individual events, a baseline amplitude was calculated as the mean of the first 0.2 ms of the event amplitude. Events that ended with a segment of at least 8.5 pA below the baseline amplitude were identified as having a terminal step. The dwell time and mean amplitude for the EBS and terminal step of each event were individually quantified.

Histograms were generated by binning the base-10 logarithm of EBS dwell time using 26 bins. Each bin represents a dwell time range from 10^n to $10^{(n+1/6)}$ ms initiating at $n = -0.5$. The dwell time probability histogram was generated by plotting each bin normalized by total number of events, revealing the fraction of events in each bin. Data from dwell times longer than 4700 ms is not displayed in the histograms for 3 mM and 10 mM dGTP because of space limitations.

Statistical analysis of the observed dwell time samples, including the number of events analyzed for each KF concentration in Table 1, for each dGTP or dTTP concentration in the text and figures, and the error estimations, are provided in Section 5 of the Supporting Information (Figure S4 and Tables S1−S3).

Acknowledgment. This work was supported by grants from Oxford Nanopore Technologies and NIGMS (GM 073617-01A1) to M.A. H.W. was partially supported by NSF (DMS 0719361). We thank Seico Benner and Felix Olasagasti for help with initial experiments, Brett Gyarfas and Noah Wilson for software development, and Daniel Branton, Andre Marziali, Matt Wiggin, and William Dunbar for comments on the manuscript.

Supporting Information Available: Figure S1 (comparison of abasic and standard DNA residues); mathematical model and derivation of mean dwell time, including Figure S2 (kinetic diagram describing the two-state model); method for determining the values of the four model parameters; results of determining the values of the four parameters; posterior analysis on the concentration of free dGTP in solution, including Figure S3 (free dGTP as a fraction of initial dGTP); statistical analysis of the observed dwell time samples, including Figures S4−S8 and Tables S−S3. This material is available free of charge via the Internet at http://pubs.acs.org.

JA809663F

(23) Li, Y.; Kong, Y.; Korolev, S.; Waksman, G. *Protein Sci.* **1998**, *7*, 1116–123.
(24) Vercoutere, W.; Akeson, M. *Curr. Opin. Chem. Biol.* **2002**, *6*, 816–822.
(25) Akeson, M.; Branton, D.; Kasianowicz, J. J.; Brandin, E.; Deamer, D. W. *Biophys. J.* **1999**, *77*, 3227–233.